

University of Groningen

Collective behavior of bulk nanobubbles produced by alternating polarity electrolysis

Postnikov, Alexander V.; Uvarov, Ilia V.; Penkov, Nikita V.; Svetovoy, Vitaly B.

Published in:
Nanoscale

DOI:
[10.1039/c7nr07126d](https://doi.org/10.1039/c7nr07126d)

IMPORTANT NOTE: You are advised to consult the publisher's version (publisher's PDF) if you wish to cite from it. Please check the document version below.

Document Version
Publisher's PDF, also known as Version of record

Publication date:
2018

[Link to publication in University of Groningen/UMCG research database](#)

Citation for published version (APA):

Postnikov, A. V., Uvarov, I. V., Penkov, N. V., & Svetovoy, V. B. (2018). Collective behavior of bulk nanobubbles produced by alternating polarity electrolysis. *Nanoscale*, *10*(1), 428-435.
<https://doi.org/10.1039/c7nr07126d>

Copyright

Other than for strictly personal use, it is not permitted to download or to forward/distribute the text or part of it without the consent of the author(s) and/or copyright holder(s), unless the work is under an open content license (like Creative Commons).

The publication may also be distributed here under the terms of Article 25fa of the Dutch Copyright Act, indicated by the "Taverne" license. More information can be found on the University of Groningen website: <https://www.rug.nl/library/open-access/self-archiving-pure/taverne-amendment>.

Take-down policy



If you believe that this document breaches copyright please contact us providing details, and we will remove access to the work immediately and investigate your claim.

Downloaded from the University of Groningen/UMCG research database (Pure): <http://www.rug.nl/research/portal>. For technical reasons the number of authors shown on this cover page is limited to 10 maximum.



Cite this: *Nanoscale*, 2018, **10**, 428

Collective behavior of bulk nanobubbles produced by alternating polarity electrolysis†

Alexander V. Postnikov,^a Ilia V. Uvarov,^a Nikita V. Penkov ^b and Vitaly B. Svetovoy *^{a,c}

Nanobubbles in liquids are mysterious gaseous objects with exceptional stability. They promise a wide range of applications, but their production is not well controlled and localized. Alternating polarity electrolysis of water is a tool that can control the production of bulk nanobubbles in space and time without generating larger bubbles. Using the schlieren technique, the detailed three-dimensional structure of a dense cloud of nanobubbles above the electrodes is visualized. It is demonstrated that the thermal effects produce a different schlieren pattern and have different dynamics. A localized volume enriched with nanobubbles can be separated from the parent cloud and exists on its own. This volume demonstrates buoyancy, from which the concentration of nanobubbles is estimated as $2 \times 10^{18} \text{ m}^{-3}$. This concentration is smaller than that in the parent cloud. Dynamic light scattering shows that the average size of nanobubbles during the process is 60–80 nm. The bubbles are observed 15 minutes after switching off the electrical pulses but their size is shifted to larger values of about 250 nm. Thus, an efficient way to generate and control nanobubbles is proposed.

Received 24th September 2017,

Accepted 2nd December 2017

DOI: 10.1039/c7nr07126d

rscl.li/nanoscale

1 Introduction

In spite of the long history of water electrolysis¹ and its applications² the process performed by short voltage pulses of alternating polarity brought many surprises.³ The Faraday current density was as high as 100 A cm^{-2} (ref. 4) while the highest value observed in ordinary DC electrolysis is 1 A cm^{-2} .⁵ Despite the high current density no visible bubbles are produced in the process⁶ although high concentration of gases in the electrolyte has been proven by different methods: a significant reduction of the refractive index of liquid⁶ and a considerable pressure increase in a closed microchamber⁷ were observed. The visible bubbles reappear in the system when a stoichiometric ratio 2 : 1 between hydrogen and oxygen is broken locally; for example, if one electrode is kept for different times at positive and at negative potential.

The high current and frequency ($\sim 100 \text{ kHz}$) of the polarity change results in an extreme supersaturation (~ 1000) with both gases in the vicinity of the electrodes.⁴ This is much

higher than the maximal value < 100 observed in DC electrolysis.⁸ The supersaturation is high enough to overcome the barrier for homogeneous nucleation of the bubbles^{9,10} that was observed under special conditions as a faint haze above the entire area of the electrodes.⁴ When the positive and negative pulses have exactly the same duration, the bubbles do not grow large and stay below 200 nm.

Direct observation of NBs is complicated by the small size and short lifetime of the objects. In the closed chamber with dimensions of $100 \times 100 \times 5 \mu\text{m}^3$ the pressure is released in $100 \mu\text{s}$ ⁷ that can be considered the typical lifetime of the bubbles. The short lifetime seems a distinctive feature of NBs produced by the alternating polarity electrochemical process, but here we will see that the bubbles can live much longer.

On the other hand, NBs produced mechanically have been actively discussed in the last decade.^{11,12} These nanoscopic gaseous domains have attracted significant attention because they live for a surprisingly long time. The theory of diffusive dissolution predicts the lifetime in the microsecond range¹³ while the NBs live for hours or even days. The reason for this exceptional stability is still under discussion. One must distinguish between surface NBs,¹² which exist at the liquid–solid interface, and the bulk NBs¹¹ existing in the liquid volume. The latter are investigated to a lesser degree, but they are relevant to this study.

Ohgaki *et al.*¹⁴ produced the bulk NBs with a rotary pump. Supersaturation with nitrogen as high as 36 was reached and water density was reduced in accordance with the gas content.

^aYaroslavl Branch of the Institute of Physics and Technology RAS, 150007 Universitetskaya 21, Yaroslavl, Russia

^bInstitute of Cell Biophysics, RAS, 142290 Pushchino, Moscow Region, Russia

^cZernike Institute for Advanced Materials, University of Groningen, 9747 AG Nijenborgh 4, Groningen, The Netherlands. E-mail: v.b.svetovoy@rug.nl;

Tel: +31 5036 34972

†Electronic supplementary information (ESI) available. See DOI: 10.1039/C7NR07126D

The bubbles were visualized using freeze-fracture replicas observed with a scanning electron microscope. The bubbles, with an average size of 100 nm, lived more than two weeks. Using a similar mechanical method to produce NBs, Ushikubo *et al.*¹⁵ measured the size distribution of oxygen NBs with dynamic light scattering (DLS). Furthermore, they measured the ζ -potential of the bubbles in the range of 20–40 mV and related the stability of NBs with the charges on their walls. An advanced theoretical model of bubble stability due to charging was developed by Yurchenko *et al.*¹⁶ Using different optical techniques, Bunkin *et al.*¹⁷ determined sizes of NBs appearing in a sodium chloride solution without external stimuli. They have been able to distinguish latex nanoparticles from NBs optically.

Bulk NBs produced by the DC electrolysis of water were described in a series of papers by Kikuchi *et al.*^{18–22} The hydrogen content of alkaline water was measured using a dissolved hydrogen meter and using the chemical method.¹⁸ The difference in the results was explained by the existence of NBs, which do not contribute to the dissolved hydrogen concentration. Independent DLS measurement supported the presence of NBs. Similar conclusions were made analyzing water from the anode chamber, which is supersaturated with oxygen.²² It was found that hydrogen NBs live a few hours while oxygen NBs live a few days.

A wide range of applications is expected for NBs. They have been applied for nanoscopic cleaning,^{23–26} for waste water treatment,^{27,28} for medical^{29–31} applications, and for heterocoagulation.^{32,33}

When the NBs are produced by alternating polarity electrolysis, the source of the bubbles is localized at the electrodes. The existence of a cloud of NBs above the electrodes was demonstrated in a recent paper.³⁴ A high concentration of gases was estimated from the optical distortion of the electrodes, but only indirect evidence that the gas is contained in the NBs was presented. In this paper, using the schlieren technique, we visualize the spatial distribution and dynamic behavior of NBs. We demonstrate that NBs can form lumps living separately from the source. Bubble size and their lifetime are measured using the DLS method.

2 Experimental

2.1 Samples and process

Electrodes are fabricated on an oxidized silicon wafer. All metallic layers are deposited by magnetron sputtering. First, a 10 nm Ti adhesion layer is deposited. Next, a 500 nm Al layer is deposited to minimize the resistance of contact lines. Finally, a 100 nm-thick working layer of titanium is sputtered. The electrodes and contact lines are patterned with the lift-off process. The contact lines are insulated with 8 μm -thick SU-8 photoresist. The wafer is diced on separate samples with sizes of $2 \times 1 \text{ cm}^2$ and $1 \times 1 \text{ cm}^2$. The concentric shape of the electrodes (see Fig. 1(a)) is chosen for the better concentration and symmetric distribution of the NBs. Titanium as a material for

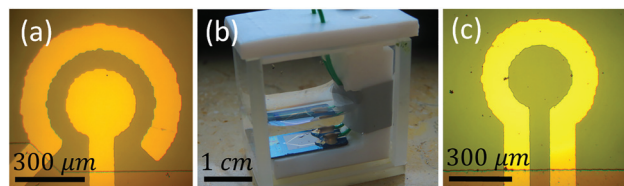


Fig. 1 (a) Titanium electrodes, the contact lines are insulated with SU-8. (b) Cuvette with a sample inside covered by a layer of the electrolyte. (c) The heating element. The chromium loop is open but the contact lines are covered with SU-8.

electrodes demonstrates stability at high current density. A disadvantage of Ti electrodes is their tendency towards oxidation, which increases the voltage applied to the electrodes.

A sample is fixed at the bottom of a cuvette (see Fig. 1(b)) with dimensions of $3 \times 2 \times 3 \text{ cm}^3$ ($l \times w \times h$). Solution of Na_2SO_4 in distilled water at a concentration of 1 mol l^{-1} is used as an electrolyte. The solution layer above the electrodes can be in the range 2–10 mm. Square voltage pulses of alternating polarity with the amplitude U and frequency f (typically $f = 200 \text{ kHz}$) are applied from the internal generator of a PicoScope 5000 and amplified by a homemade amplifier (see Fig. S1†). The typical voltage used in this experiment is 11 V. The pulses can be generated continuously with a constant amplitude or with the amplitude modulated by a triangle profile. The voltage, current through the cell, and triggering pulses for camera are recorded by the PicoScope.

2.2 Schlieren setup

The lens and grid schlieren technique³⁵ is used in this work to visualize the variation of the optical density induced by the electrochemical process. The system uses a one dimensional array (grid) of light sources instead of a point source in the conventional schlieren system. The source grid is imaged with an objective onto a one-dimensional array of corresponding knife-edge cutoffs. The grid is a series of alternating opaque and transparent stripes. The cutoff grid is a photographic negative image of the source grid. The system is shown schematically in Fig. 2. It can be thought of as the superposition of many conventional schlieren systems, with each transparent stripe of the source grid and corresponding opaque stripe of the cutoff grid functioning as the light source and knife edge, respectively.³⁶

To increase the sensitivity, the transparent stripes in the source grid have to be narrow, but the diffraction effects may become important blurring the image.³⁵ The field of view is limited by the source grid and viewing angle. If the numerical aperture of the imaging lens is large enough, the system will have a narrow depth of focus and such a system is described as a focusing schlieren system. The orientation of the grids (horizontal or vertical) depends on the desired direction of sensitivity.

The source grid of our schlieren setup consists of a series of 400 μm opaque stripes separated by 100 μm transparent gaps.

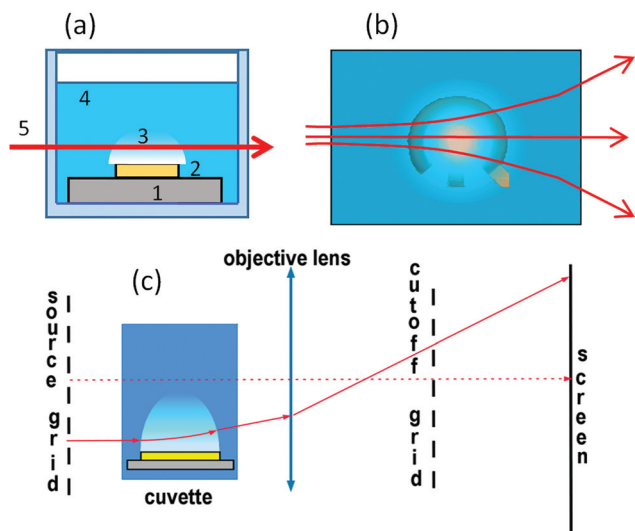


Fig. 2 Scheme of the schlieren experiment. (a) Sample in the cuvette (side view). Substrate, electrodes, cloud of NBs, electrolyte, and light beam passing through the cloud are numbered from 1 to 5, respectively. (b) Top view on the electrodes covered with the cloud of NBs. Refraction of the light beam is shown. (c) Scheme of the lens and grid schlieren setup.

For the cutoff grid, the stripes are inverted. The grids are 40 mm in diameter quartz substrates sputtered with a 100 nm-thick chromium layer. The substrate is patterned with standard lithography. The cuvette with electrolyte is positioned between the source grid and the lens. A lens with a 50 mm focal length and 25 mm aperture is used to image inhomogeneities of the optical density. To increase the field of view we use also a lens with a focal distance of 150 mm. The grids are aligned with a horizontal microscope. If the system is properly adjusted the sensor is illuminated uniformly. The cutoff grid is aligned so that the regions of lower refraction become darker and the regions of higher refraction become brighter compared to the background. Space resolution of our system in the test section can be estimated from the image blur as 20 μm for the short focus lens (50 mm) and 70 μm for the long focus lens (150 mm).

2.3 Thermal effect

The temperature of the electrolyte during the process is measured with a copper-constantan thermocouple. For insulation, the wires and the junction (200 μm in size) are covered with a compound OMNIVISC 1050 (thickness of 10–20 μm).

A special heater (see Fig. 1(c)) has been fabricated on silicon substrate to mimic the Joule heating produced by the current in the electrochemical process. The heater is a 100 nm-thick chromium loop that has the same shape as the gap between the electrodes. The resistance of the loop is 3.63 Ω at 27 $^{\circ}\text{C}$. The contact lines are covered by 8 μm of SU-8 photoresist and the total resistance of the heating element is 14 Ω . The thermal coefficient $\alpha = 2.4 \times 10^{-3} \text{ C}^{-1}$ of the heater was found by measuring the resistance in distilled hot water.

The heater has four contact lines that allows the voltage application and the measurement of the voltage drop on the loop independently.

2.4 Dynamic light scattering

The size distribution of the NBs is determined using the dynamic light scattering method. The measurement is made with a Zetasizer nano ZS analyzer (Malvern, UK). The samples are placed in a polystyrene cuvette with a cross-section of $10 \times 10 \text{ mm}^2$. The cuvette is filled with the electrolyte. The laser beam (wavelength 633 nm) has a Gaussian width of 0.1 mm. The scattering angle is fixed and equal to 173° (backscattering).

The electrolyte was thoroughly filtered by a filter with an average pore diameter of 200 nm before use. We only took measurements if the solution did not demonstrate any particles before bubble generation. The bubbles are generated at a distance of 5–7.5 mm from the bottom of the cuvette and the laser beam passes 8 mm above the bottom. Due to instrument design, it is difficult to precisely control the position of the beam above the electrodes. For this reason, the beam might not be in the optimal position (above the central electrode), but blind shifts of the cuvette within 2 mm do not change the signal significantly.

The measurements are taken as follows. First, the electrolyte before bubble generation is measured to check the absence of external nanoparticles in the solution. Then, the bubbles are generated for 2 min by applying continuous voltage pulses with an amplitude of 8–12 V at frequencies of 150 and 325 kHz. One measurement is taken during the generation. When the electrical pulses are switched off, a few more measurements are taken during 15 min after the generation.

3 Results and discussion

3.1 Faraday current

If a DC voltage or single polarity pulses are applied to the electrolytic cell, one electrode is oxidized quickly and the process stops, leaving a few visible gas bubbles. When alternating polarity pulses are applied, a significant current is flowing through the electrolyte as shown in Fig. 3, but no visible gas is observed. In this case, an oxide layer is formed on one electrode over half of the period, but then reduced over the second half. In contrast with such metals as Pt, Cu, or W the current contains not only the charging–discharging and Faraday components,⁴ but also includes the oxidation–reduction component. For this reason, the Faraday current I_F cannot be extracted from each pulse using a simple 3-parametric fit $I(t) = I_F + I_1 e^{-t/\tau}$ as was done in ref. 4, where τ is the relaxation time for the charging–discharging process. For each pulse, the function $I(t)$ is not concave, revealing the presence of the oxidation–reduction component. Due to this complication, we roughly estimate the Faraday current using a different procedure.

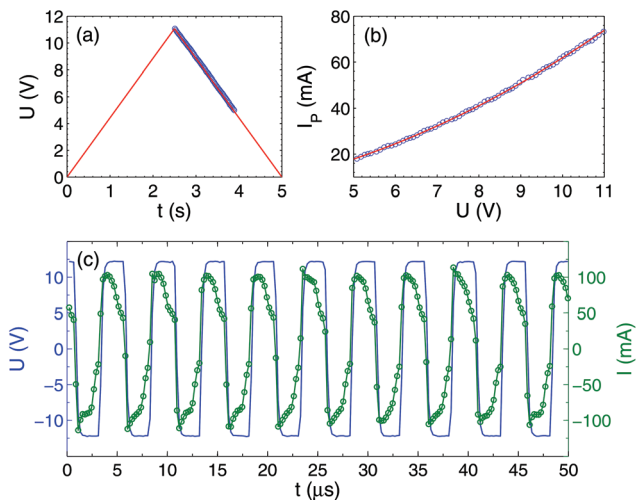


Fig. 3 Voltage and current through the cell. (a) Amplitude of applied voltage pulses as a function of time. Blue circles mark the time interval, where high-resolution data were collected. (b) The current is determined from the power (see text) as a function of applied voltage amplitude U . (c) Time-resolved voltage (left axis) and current (right axis) pulses. The open circles show the actual sampling.

First, from the time-resolved data, we determine the consumed power $P(U)$ averaged over 10 periods at a fixed amplitude of the voltage pulses U . From this power, we extract the current $I_p = P/U$ shown in Fig. 3(b). It can be fitted by the following non-linear curve $I_p = 64.2(U/U_0)^2 + 10.5(U/U_0)$ mA, where $U_0 = 11$ V is the maximal amplitude. The Faraday current gives the main contribution to I_p . We define it as $I_F = kI_p$, where the coefficient k is estimated roughly as $k = 0.67$ based on the observation that both the charging–discharging and the oxidation–reduction processes are faster than the pulse duration. Thus, at $U = U_0$ the Faraday current is estimated as $I_F = 50$ mA. It is close to the value $I_F = 60$ mA reported for a similar but different sample.³⁴ The Faraday current density is estimated as $j_F = 70$ A cm⁻² which is at the same level as for all alternating polarity experiments.³ It is worth noting that the slightly-nonlinear behavior $I_p(U)$ is not related to the effect of heating of the electrolyte, because a direct measurement of the temperature rise is less than 10 °C (see below). This systematically observed effect for Ti electrodes (but not for Pt, Cu, or W) is apparently related to the slow decrease of the thickness of the oxide layer on the Ti surface during the process.

Although no visible bubbles are produced by the alternating polarity process, significant Faraday current means that gas is generated. Absence of bubbles scattering visible light apparently is related to the reaction between gases that does not allow bubbles to grow large. The generated gas has to change the optical density of the medium near the electrodes. Using our schlieren setup we visualize how the optical density is distributed in space and time.

3.2 Optical density

Square voltage pulses at frequency $f = 200$ kHz modulated by a triangle waveform with a period of 5 s are applied to the cell.

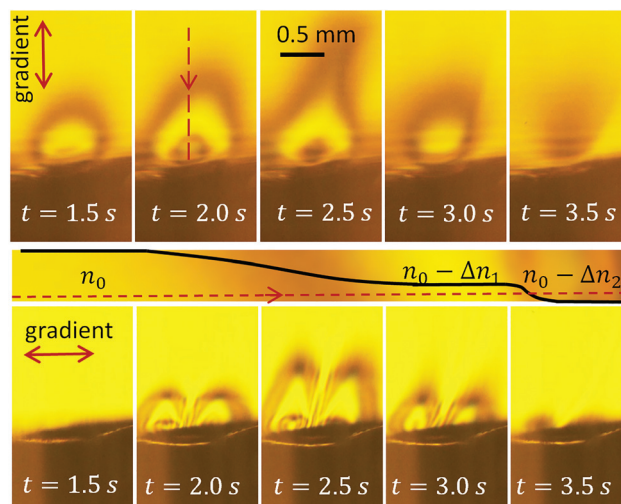


Fig. 4 Schlieren contrast produced by the alternating polarity process. The upper row (frames from Video S1†) shows the vertical gradient of the optical density. The stripe below the images schematically explains the formation of the contrast along the red dashed line in the image at $t = 2.0$ s (see the text). The lower row of images presents the gradient in the horizontal direction.

The maximum voltage amplitude is $U_0 = 11$ V. The schlieren contrast is shown in Fig. 4 (see also Video S1†). The upper row of images demonstrates successive changes of the gradient of optical density in the vertical direction. The lower row shows the changes in the horizontal direction.

Similar to the classical schlieren method, our setup is sensitive to the gradient of the refractive index in the medium in the direction normal to the knife edge. The vertical gradient is resolved at $U > 4.5$ V. The region near the electrodes becomes darker – as it should be for a liquid enriched with gas. When the voltage amplitude increases further, the area of lower refraction grows and the central part becomes bright again, as one can see in the frame at $t = 1.5$ s. In its central part, the refraction index is smaller than in the background liquid but homogeneous. Since there is no gradient, we see this region at the same level of brightness as the background. The region of lower refraction forms a cloud of optically-less-dense liquid covering the electrodes.

In the frames corresponding to $t = 2.0$ s and 2.5 s, a dark spot is visible in the center of the cloud. It originates from nonhomogeneous current density distribution, which is the largest at the edge of the central electrode, somewhat smaller in the center, and the smallest at the peripheral electrode. Because of this distribution, the optical density above the central electrode is even smaller than in the main part of the cloud. This is clear from the fact that we see it dark again. If this region were optically more dense, we would see a bright spot – not a dark one. With increasing voltage, the area of smaller optical density increases, but at the maximum voltage $U = 11$ V at $t = 2.5$ s, one can see that the cloud develops a neck. This is an interesting phenomenon that will be discussed separately. One can notice that the neck is not exactly

vertical. This is explained by uncontrolled convection of likely thermal origin. When the voltage decreases, the system goes *via* the same states in the opposite direction. The contrast formation is explained schematically in the stripe panel below the upper row of images in Fig. 4.

The lower row of images demonstrates the approximate reflection symmetry of the electrodes. A ray passing through the center of the structure does not deviate, but the ray passing left from the center deviates to the left from its original direction and the one passing right from the center deviates to the right as one can see in Fig. 2(b). The images at $t = 2.0$ s and $t = 2.5$ s have a darker spot in the center of the left and right halves, related to the higher concentration of gas near the edge of the central electrode.

From Fig. 4, we can conclude that the application of the alternating polarity voltage pulses produces gas above the electrodes that does not form bubbles strongly scattering the visible light but reduces the refractive index of the liquid. This gas is distributed in the form of a dome covering the electrodes. The gas concentration within the dome is the same nearly everywhere, although it is higher and distributed inhomogeneously near the central electrode. At higher voltage amplitude, the dome develops a neck. Now we are going to discuss the origin of this neck.

To see the area above the neck, we use an objective with a 150 mm focal length. It enlarges the field of view. The same pulses at 200 kHz modulated by the triangle waveform are used. Fig. 5 shows a few frames with schlieren contrast from Video S2.† As the initial moment $t = 0$ we take the state with the maximum voltage amplitude. The upper row shows a series of images taken with a time step of 0.5 s. We can see

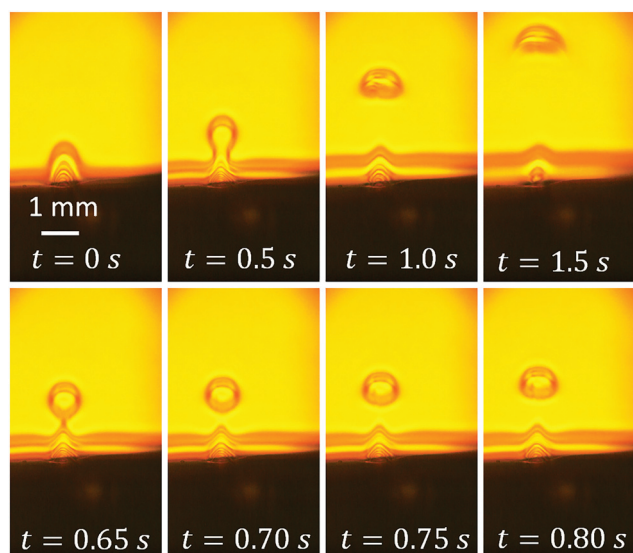


Fig. 5 Schlieren contrast (frames from Video S2†) for a larger field of view in comparison with Fig. 4. Upper row shows successive images separated by a time of 0.5 s. In the lower row, the evolution of the gas-enriched “drop” is shown on the shorter time scale. The moment $t = 0$ corresponds to the maximum voltage.

that initially, the cloud with a lower refraction index is attached to the substrate as in Fig. 4. Then, a volume of spherical shape is separated from the parent cloud while still tied to it by the neck. This separated volume enriched with gas resembles a “drop” of liquid with a smaller mass density than the surrounding liquid. In contrast to a normal drop, it has no sharp boundary. In the next image at $t = 1.0$ s, the “drop” is completely detached and rising up to the free surface of the liquid. In the last image of the upper row, one can see that the “drop” changes its shape during rising as would a normal drop of lighter liquid or a bubble. When the “drop” reaches the free surface, the gas does not go out to the atmosphere but spreads along the free surface as one can see in Fig. S2.†

In the lower row, four successive images (time step is 50 ms) are shown. They demonstrate how the “drop” rises up, preserving its shape on this short time scale. From the last three images at $t = 0.70$, 0.75 and 0.80 s, one can estimate the rising velocity as $v = 2.8 \text{ mm s}^{-1}$ and the “drop” radius as $R = 315 \text{ }\mu\text{m}$. Physically, what we have here is a nearly-spherical volume enriched with gas. The mass density in this volume is smaller than the density in the background liquid. Therefore, the “drop” has to be subjected to buoyancy, which explains its rise. When the sample is mounted parallel to the gravity direction, one can see that we are really dealing with a buoyancy force (see Fig. S3†).

3.3 Thermal effect

Alternatively, the observed contrast could be generated by a nonhomogeneous temperature distribution around the electrodes. The current flowing through the electrolyte produces Joule heat that can change the refractive index of the liquid. Direct measurement of the temperature rise near the electrodes with the thermocouple gives a maximum value of $\Delta T = 10 \pm 1 \text{ }^\circ\text{C}$ just above the central electrode. No temperature change is found at a distance of 3 mm from the center of the electrodes in any direction.

To see how the temperature distribution influences the schlieren contrast, we observe the contrast produced by the heater (see Fig. 1(c)) in distilled water. Applying a triangle voltage from 0 to 7.9 V with a period of 2 s, we observe the contrast presented in Video S3.† A few frames from this video are shown in Fig. 6. The temperature rise of the heater loop is estimated as $\Delta T = 9.5 \text{ }^\circ\text{C}$ at maximum voltage. The maximum power dissipated by the loop is $P_1 = 0.9 \text{ W}$, which is close to the power $P_{e1} = 0.8 \text{ W}$ dissipated in the electrochemical process.

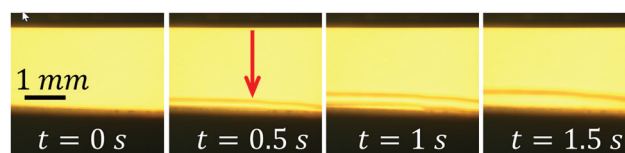


Fig. 6 The thermal contrast (frames from Video S3†). The arrow in the second image indicates the position of the heater center. Triangle voltage with a period of 2 s is applied to the heater.

The total maximum power of the heater $P_{\text{tot}} = 4.4$ W is larger due to the heat produced by the contact lines. These lines also make a contribution to the contrast, although the extra power is dissipated far from the loop.

One can see the completely different character of the thermal contrast. The region with lower optical density is broader in the horizontal direction, but does not go far from the substrate in the vertical direction. The latter is related to the high heat conductivity of the silicon substrate. The observed movement of the contrast is explained by the convection along the substrate. It must be noted that there is no preferable direction of the convection that is randomly defined from run to run. Now we can relate a part of the contrast observed during the electrolysis with the thermal effect. In Video S2† (see also Fig. 5), one can see that with the voltage increase and decrease, the contrast concentrated in the layer above the substrate appears and disappears.

3.4 Size of the bubbles

We have already established that the optical contrast appears due to liquid enriched with gas. This gas has to form bubbles, whose sizes can be determined using light scattering. The bubbles, of a size comparable to the wavelength of visible light, can be easily identified due to the strong scattering of light. However, we do not observe these bubbles independently on the generation or observation time. Therefore, one would expect that the gas that manifests itself as the optical contrast has to form NBs. The latter weakly scatter the light, but their size can be determined using the DLS method.

Investigation of light scattering with a Zetasizer nano ZS analyzer reveals that the NBs are indeed generated by the alternating polarity process. After careful filtering of the solution, the analyzer does not identify any nanoparticles in the solution. When the electrical pulses are switched on, we observe bubbles with the diameter in the range of 50–90 nm. After switching off the pulses the signal becomes weaker and disappears in 15 min. What is interesting is that the bubble sizes that are observed after the process lie in the range of 200–300 nm. They are larger and their distribution is broader than those during the process. The change in the sizes occurs faster than the time needed to collect the signal (~ 1 min), such that we are unable to see the transition.

Some results are presented in Fig. 7. In panel (a), two different runs for the same voltage amplitude $U = 11$ V and frequency $f = 150$ kHz are shown. These two runs demonstrate the reproducibility of the size distribution. The peak at smaller bubble diameter is found during the process and the peak at larger diameter corresponds to the measurement that is taken 3 min after the process. Panel (b) shows the signal for $U = 11.5$ V and $f = 325$ kHz. In this case, the bubbles are slightly smaller but have very similar widths of distribution. With the available data, we cannot draw the definite conclusion that the bubble size depends on frequency.

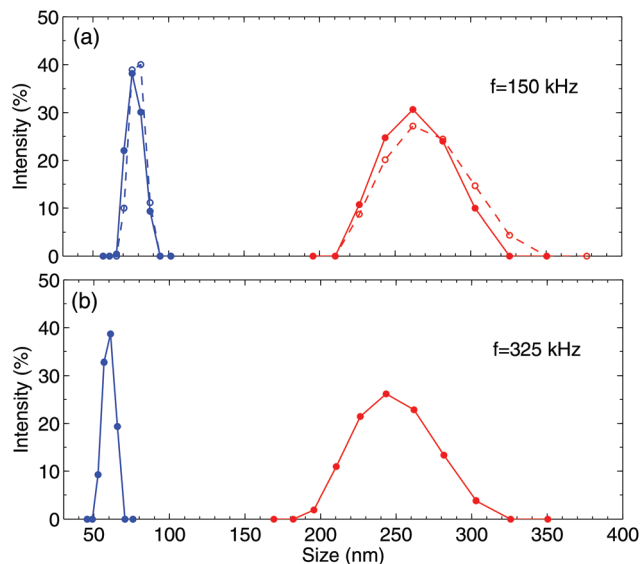


Fig. 7 Size distribution of NBs. The blue curves (smaller sizes) correspond to the data collected when the electrical pulses are switched on. The red curves show the size distribution 3 min after switching off the pulses. Panels (a) and (b) show the data collected for the different frequencies of the pulses.

3.5 Discussion

Our results demonstrate that the alternating polarity electrochemical process generates NBs around the electrodes. No microbubbles strongly scattering the visible light are formed in contrast with normal DC electrolysis. Although we do not identify the gases responsible for the change in optical density, the significant Faraday current shows that these gases are hydrogen and oxygen. According to the Faraday law, the total number of gas molecules produced during a 5-second cycle is

$$N = \frac{3}{4|e|} \int_0^{t_0} I_F(t) dt \approx 4 \times 10^{17}, \quad (1)$$

where $t_0 = 5$ s is the period of the triangle modulation and e is the charge of the electron. Even if all this gas were to be homogeneously distributed in the electrolyte (total volume of about 1 ml), the liquid would be supersaturated with both gases after just one cycle.

In reality, most of the gas is concentrated near the electrodes, providing the contrast presented in Fig. 4. Although with our schlieren setup we cannot estimate the gas concentration in the cloud, one can do this with the optical distortion method. In this experiment, when the sample is observed from the top, we see the optical distortion of the electrodes visible to the naked eye. This effect was described earlier³⁴ and the gas concentration responsible for the distortion was estimated. In this experiment the number of gas molecules produced by the process is 2–3 times smaller and we expect the gas concentration in the cloud to be as high as $n_g \sim 1 \times 10^{26} \text{ m}^{-3}$.

The lump of NBs (“drop”) that is separated from the parent cloud rises up because it has a smaller mass density than the surrounding liquid. We can estimate the volume fraction of gas f_g in the “drop” using as input parameters the radius of the “drop” R and its velocity v . Equating the buoyancy force and the Stokes’ drag acting on the “drop” one finds for the total gas fraction (hydrogen + oxygen)

$$f_g = \frac{9\eta v}{2(\rho_l - \rho_g)gR^2}, \quad (2)$$

where ρ_l and ρ_g are the densities of liquid and gas, respectively, g is the free-fall acceleration, and η is the viscosity of the solution. From this expression, we find $f_g \approx 0.013$. Since the lump exists separately from the parent cloud, it has to be composed of larger NBs with a size of 250 nm. Calculating the total number of gas molecules N in the “drop” with the help of the ideal gas law, one finds for the gas concentration $n_g \approx 4 \times 10^{24} \text{ m}^{-3}$. It is much smaller than that in the parent cloud, since the “drop” is not supported by the gas produced by the electrodes. Additionally, the “drop” is composed from larger NBs that have smaller Laplace pressure.

Observation of different sizes of NBs during and after the electrochemical process can be explained by Ostwald ripening. The cloud is composed of densely packed hydrogen and oxygen NBs. The concentration of NBs is $n_{\text{NB}} = n_g/N_r$, where N_r is the number of gas molecules in one NB. The latter can be estimated using the ideal gas law. Thus, for $n_g = 1 \times 10^{26} \text{ m}^{-3}$ and for the average bubble radius $r = 40 \text{ nm}$, one finds $n_{\text{NB}} = 4 \times 10^{20} \text{ m}^{-3}$. For this concentration of NBs, the average distance between the bubble centers is estimated as 140 nm, so that the bubbles are separated only by a distance of 60 nm. At such a small separation, the bubbles exchange rapidly by the content *via* the gas diffusion in liquid. If two neighboring bubbles have the same gas, one bubble disappears while the other one grows. If the gases in the neighboring bubbles are different, then one bubble disappears but the other one becomes smaller. This is due to the combustion reaction between hydrogen and oxygen that happens in NBs spontaneously at room temperature.⁶ A steady state in bubble distribution within the cloud is supported by the gas produced by the electrodes.

When the electrochemical process is switched off, the size distribution is shifted to larger values and the total gas concentration is reduced. We observe the NBs 15 min after switching off the process. This time is much longer than the time $\sim 1 \text{ ms}$ needed for the diffusive dissolution of a 250 nm bubble.¹³ On the other hand, it is shorter than the lifetime of bulk NBs produced mechanically (days)^{14,15} or by normal electrolysis (hours).¹⁸ The shorter lifetime of NBs in our experiment is explained not by the different physical properties of the bubbles, but rather by the possibility of the gases to interact: occasionally two NBs with different gases can meet and disappear in the reaction.

The lump of NBs separated from the parent cloud is not supported by the gas from the electrodes. For this reason, it

has to contain larger NBs with an average size of 250 nm. The concentration of NBs in the “drop” is estimated as $n_{\text{NB}} = 2 \times 10^{18} \text{ m}^{-3}$ and the average distance between them equal to 0.8 μm is much larger than that in the parent cloud.

4. Conclusions

We generated a dense cloud of H_2 and O_2 nanobubbles that was controlled in space and time. This was achieved using the electrochemical decomposition of water with short voltage pulses of alternating polarity. The process produces only small NBs that do not scatter strongly the visible light. The detailed structure of the cloud was investigated using the collective effects produced by the NBs. The significant fraction of the gas in the liquid was visualized using a lens-and-grid schlieren setup. The NBs formed a dome-shaped cloud covering the concentric electrodes. Inside of the dome, the NBs are distributed inhomogeneously in correspondence with the current density distribution.

We observed the separation of a lump of NBs from the parent cloud. The lump takes a spherical shape and rises up to the free surface, changing its shape along the way. A single NB has negligible buoyancy, but the lump was moved as a whole by gravity since it has smaller mass density than the surrounding liquid. From this movement, we estimated the density of the NBs in the lump as $2 \times 10^{18} \text{ m}^{-3}$, which is considerably smaller than that in the parent cloud.

Using dynamic light scattering, we determined the size and lifetime of the NBs in the cloud. This makes the first direct measurement of the sizes of NBs in the alternating polarity electrochemical process. While the electrical pulses were switched on, the average size of the bubbles was found to be 60–80 nm, but when the pulses were switched off, the distribution became broader and shifted to larger values around 250 nm. These bubbles can be observed 15 minutes after the process has been terminated. The change in the distribution and concentration of NBs during and after the electrochemical process was related to the spontaneous combustion reaction between hydrogen and oxygen in the NBs.

Conflicts of interest

There are no conflicts to declare.

Acknowledgements

This work is supported by the Russian Science Foundation, Grant No. 15-19-20003.

References

- 1 R. de Levie, *J. Electroanal. Chem.*, 1999, **476**, 92–93.

- 2 K. Zeng and D. Zhang, *Prog. Energy Combust. Sci.*, 2010, **36**, 307–326.
- 3 V. Svetovoy, A. Postnikov, I. Uvarov, R. Sanders and G. Krijnen, *Energies*, 2016, **9**, 94.
- 4 V. B. Svetovoy, R. G. P. Sanders and M. C. Elwenspoek, *J. Phys.: Condens. Matter*, 2013, **25**, 184002.
- 5 H. Vogt and R. Balzer, *Electrochim. Acta*, 2005, **50**, 2073–2079.
- 6 V. B. Svetovoy, R. G. P. Sanders, T. S. J. Lammerink and M. C. Elwenspoek, *Phys. Rev. E: Stat., Nonlinear, Soft Matter Phys.*, 2011, **84**, 035302(R).
- 7 V. B. Svetovoy, R. G. P. Sanders, K. Ma and M. C. Elwenspoek, *Sci. Rep.*, 2014, **4**, 4296.
- 8 H. Vogt, *J. Appl. Electrochem.*, 1993, **23**, 1323–1325.
- 9 P. G. Debenedetti, *Metastable liquids: Concept and Principles*, Princeton University Press, New York, 1996.
- 10 V. P. Skripov, *Metastable liquids*, John Wiley, New York, 1974.
- 11 M. Alheshibri, J. Qian, M. Jehannin and V. S. J. Craig, *Langmuir*, 2016, **32**, 11086–11100.
- 12 D. Lohse and X. Zhang, *Rev. Mod. Phys.*, 2015, **87**, 981–1035.
- 13 P. S. Epstein and M. S. Plesset, *J. Chem. Phys.*, 1950, **18**, 1505–1509.
- 14 K. Ohgaki, N. Q. Khanh, Y. Joden, A. Tsuji and T. Nakagawa, *Chem. Eng. Sci.*, 2010, **65**, 1296–1300.
- 15 F. Y. Ushikubo, T. Furukawa, R. Nakagawa, M. Enari, Y. Makino, Y. Kawagoe, T. Shiina and S. Oshita, *Colloids Surf., A*, 2010, **361**, 31–37.
- 16 S. O. Yurchenko, A. V. Shkirin, B. W. Ninham, A. A. Sychev, V. A. Babenko, N. V. Penkov, N. P. Kryuchkov and N. F. Bunkin, *Langmuir*, 2016, **32**, 11245–11255.
- 17 N. F. Bunkin, A. V. Shkirin, P. S. Ignatiev, L. L. Chaikov, I. S. Burkhanov and A. V. Starosvetskij, *J. Chem. Phys.*, 2012, **137**, 054707.
- 18 K. Kikuchi, H. Takeda, B. Rabolt, T. Okaya, Z. Ogumi, Y. Saihara and H. Noguchi, *J. Electroanal. Chem.*, 2001, **506**, 22–27.
- 19 K. Kikuchi, Y. Tanaka, Y. Saihara and Z. Ogumi, *Electrochim. Acta*, 2006, **52**, 904–913.
- 20 K. Kikuchi, Y. Tanaka, Y. Saihara, M. Maeda, M. Kawamura and Z. Ogumi, *J. Colloid Interface Sci.*, 2006, **298**, 914–919.
- 21 K. Kikuchi, S. Nagata, Y. Tanaka, Y. Saihara and Z. Ogumi, *J. Electroanal. Chem.*, 2007, **600**, 303–310.
- 22 K. Kikuchi, A. Ioka, T. Oku, Y. Tanaka, Y. Saihara and Z. Ogumi, *J. Colloid Interface Sci.*, 2009, **329**, 306–309.
- 23 Z. Wu, H. Chen, Y. Dong, H. Mao, J. Sun, S. Chen, V. S. Craig and J. Hu, *J. Colloid Interface Sci.*, 2008, **328**, 10–14.
- 24 G. Liu, Z. Wu and V. S. J. Craig, *J. Phys. Chem. C*, 2008, **112**, 16748–16753.
- 25 G. Liu and V. S. J. Craig, *ACS Appl. Mater. Interfaces*, 2009, **1**, 481–487.
- 26 J. Zhu, H. An, M. Alheshibri, L. Liu, P. M. J. Terpstra, G. Liu and V. S. J. Craig, *Langmuir*, 2016, **32**, 11203–11211.
- 27 T. Tasaki, T. Wada, Y. Baba and M. Kukizaki, *Ind. Eng. Chem. Res.*, 2009, **48**, 4237–4244.
- 28 A. Agarwal, W. J. Ng and Y. Liu, *Chemosphere*, 2011, **84**, 1175–1180.
- 29 S. Mondal, J. A. Martinson, S. Ghosh, R. Watson and K. Pahan, *PLoS One*, 2012, **7**, e51869.
- 30 K. K. Modi, A. Jana, S. Ghosh, R. Watson and K. Pahan, *PLoS One*, 2014, **9**, e103606.
- 31 J. Owen, C. McEwan, H. Nesbitt, P. Bovornchutichai, R. Averre, M. Borden, A. P. McHale, J. F. Callan and E. Stride, *PLoS One*, 2016, **11**, 1–12.
- 32 N. Mishchuk, J. Ralston and D. Fornasiero, *J. Colloid Interface Sci.*, 2006, **301**, 168–175.
- 33 A. Azevedo, R. Etchepare, S. Calgaroto and J. Rubio, *Miner. Eng.*, 2016, **94**, 29–37.
- 34 A. V. Postnikov, I. V. Uvarov, M. V. Lokhanin and V. B. Svetovoy, *PLoS One*, 2017, **12**, 1–18.
- 35 L. Weinstein, *Eur. Phys. J.: Spec. Top.*, 2010, **182**, 65–95.
- 36 D. Floryan, J. Hofferth and W. Saric, *Design, assembly, and calibration of a focusing schlieren system*, Cornell university, ithaca technical report, 2012.